Modeling and Performance Analysis of Differential CQI Feedback in OFDM Cellular Systems

Vineeth Kumar and Neelesh B. Mehta, *Senior Member, IEEE*

***Abstract*—Reduced feedback schemes play a critical role in contemporary orthogonal frequency division multiplexing systems such as Long Term Evolution (LTE). They ensure that the channel state information required for downlink rate adaptation and scheduling is available at the base station (BS) without overwhelming the uplink with feedback overhead. We present a novel model and analysis of the single-user and multi-user throughput of the widely used differential feedback scheme of LTE, which is called eNodeB-configured subband feedback. In it, a user feeds back a 2-bit differential channel quality indicator (CQI) for each subband relative to a 4-bit wideband CQI, which indicates the rate that the user can decode if the BS were to transmit over the entire system bandwidth. Our analysis applies to many multi-antenna modes. In addition to bringing out several insights, it shows that differential feedback can reduce the feedback overhead significantly while incurring only a marginal reduction in throughput.**

***Index Terms*—OFDM, differential feedback, rate adaptation, scheduling**

I. Introduction

Contemporary wireless communication standards such as 4G Long Term Evolution (LTE) use orthogonal frequency division multiplexing (OFDM) in the downlink [1]. OFDM is also likely to be used in 5G. Frequency-domain scheduling and adaptive modulation and coding (AMC) are two key techniques employed in such OFDM systems to enhance the spectral efficiency [1]. Reduced feedback schemes play a crucial role in these systems by providing the base station (BS) with the requisite channel state information (CSI) from every user about each orthogonal subchannel (SC) while ensuring that the uplink is not overwhelmed by the feedback overhead. Several reduced feedback schemes have been proposed in the literature and adopted in the standards [2]. We summarize the most pertinent schemes below.

A. Reduced Feedback Schemes Used in OFDM Systems

Threshold-based quantized feedback, best-m feedback, SC clustering-based feedback, and differential feedback are among the popular feedback schemes used in OFDM systems [2]–[4]. In best-m feedback, each user sorts the signal-to-noise-ratios (SNRs) of the SCs and reports the indices and the corresponding rates for m SCs that can support the highest rates [3], [4]. In SC clustering-based feedback, adjacent SCs are grouped into clusters and feedback is sent only for each cluster [5]. Differential feedback schemes further reduce the feedback overhead by feeding back only the difference between a reference value and the quantity to be fed back.

LTE employs a combination of the schemes mentioned above [1]. In LTE, a user feeds back a channel quality indicator (CQI), which indicates the modulation and coding scheme (MCS) that it can decode reliably. In *wideband feedback*, a user reports just a single wideband CQI. It is the MCS that can be reliably decoded if the entire system bandwidth is allocated to that user. However, this scheme cannot support frequency-domain scheduling at the BS since different SCs can see different fades. To support such scheduling, the following two schemes are used, which feed back more information in addition to the wideband CQI. In *UE-selected subband feedback*, indices of the best-m subbands, where each subband comprises several adjacent SCs, and a wideband CQI over the reported subbands is sent. In *eNodeB-configured subband feedback*, a 2-bit differential CQI that encodes the difference between the wideband CQI and the MCS that the user can receive reliably on the subband is sent for each subband.

B. Focus and Contributions

In this paper, we present a novel and systematic modeling and analysis of the widely used eNodeB configured subband feedback scheme of LTE, which employs differential feedback. Our analysis is novel and differs from prior works that have been simulation-based [6], [7], which makes it difficult to generalize their results and conclusions. It is comprehensive because it takes into account the impact of frequency-domain scheduling at the BS and the different multiple antenna diversity modes that are employed in LTE. It is relevant as it gives rigorous mathematical insights about the performance of the scheme. Furthermore, it enables a system designer to independently evaluate or verify the throughput of the scheme over a wide range of system parameter settings without resorting to computationally intensive simulations.

We make the following contributions:

- We derive the expression for the throughput of the differential feedback scheme in a single-user scenario and in a multi-user scenario with the round-robin (RR) scheduler. We do so for the case when the subband SNRs of a user are independent and identically distributed (i.i.d.), which is justified when the coherence bandwidth of the channel is comparable to the bandwidth of a subband. Our results apply to several multi-antenna modes such as single-input-single-output

V. Kumar and N. B. Mehta are with the Dept. of Electrical Communication Eng. (ECE), Indian Institute of Science (IISc), Bangalore, India (Emails: vineethkumar01@gmail.com, neeleshbmehta@gmail.com).

This research was partially supported by a project funded by the Ministry of Communication & Information Technology and the DST Swarana Jayanti Fellowship award DST/SJF/ETA-01/2014-15.

978-1-5386-3180-5/18/$31.00 ©2018 IEEE

(SISO), single-input-multiple-output (SIMO), multiple-input-single-output (MISO), and single-stream multiple-input-multiple-output (MIMO).

- A key aspect of our approach is the modeling of the wideband CQI using the exponential effective SNR mapping (EESM). Another important aspect is the development of an accurate model for the joint statistics of EESM and the differential CQI, which drives the performance of the scheme. EESM is a widely used link quality metric that can be interpreted as the equivalent SNR that the codeword sees if it were transmitted over a flat-fading channel. It enables us to employ techniques used for analyzing classical link adaptation over flat-fading channels to this more involved model.
- To study the effect of correlation between the subband SNRs, we also derive the throughput expressions for the alternate, extreme scenario in which the subband SNRs are correlated with a correlation coefficient equal to 1. As we show, this scenario also helps quantify the marginal loss in throughput due to the markedly less feedback overhead of the differential feedback scheme.

C. Organization and Notation

The system model is described in Section II. Section III first analyzes the throughputs of the single-user and multi-user scenarios. Numerical results are presented in Section IV. Our conclusions follow in Section V.

Notation: We denote the probability of an event A by $\Pr(A)$ and the joint probability of events A and B by $\Pr(A, B)$. The conditional probability of A given B is denoted by $\Pr(A \mid B)$. The probability density function (PDF) and cumulative distribution function (CDF) of a random variable (RV) X are denoted by $f_X(\cdot)$ and $F_X(\cdot)$, respectively. We denote the expectation with respect to RV X by $\mathbb{E}_X[\cdot]$, and the absolute value by $|\cdot|$.

II. System Model

We study the following system model that captures several important aspects of LTE. We consider an OFDM-based cellular system with one BS serving K users. The BS has N_t transmit antennas and each user has N_r receive antennas. The system bandwidth is divided into N_{PRB} orthogonal physical resource blocks (PRBs). Groups of q adjacent PRBs form subbands [1]. Hence, the total number of subbands is $N_{\text{SB}} = \lceil N_{\text{PRB}}/q \rceil$, where $\lceil \cdot \rceil$ denotes the ceiling function.

We focus on the single-cell scenario for the following reasons: (i) It has received considerable attention in the literature [3], [8], [9]. (ii) No analysis of the differential feedback scheme is available in the literature even for it.

Channel Model: We model the channel between a user and the BS as a frequency-selective Rayleigh fading channel. Let $H_{kn}(i,j)$ denote the complex baseband gain of downlink subband n for user k between the i^{th} transmit antenna of the BS and the j^{th} receive antenna of the user. The fade is assumed to remain constant over a subband. This is justified when the bandwidth of a subband, which ranges from 360 kHz to 1.4 MHz, is comparable to the coherence bandwidth of the channel. For instance, for the typical urban (TU) channel, the coherence bandwidth is 530 kHz. $H_{kn}(i,j)$ is a circularly symmetric complex Gaussian RV with zero mean and variance $\delta x_k^{-\alpha}$, where α is the path loss exponent, δ is a path loss constant, and x_k is the distance between user k and the BS [10, Chap. 2]. The subband power gains $|H_{kn}(i,j)|^2$ of user k are statistically identical, which follows from the uncorrelated scatterers assumption [10, Chap. 3]. The subband power gains of different users are statistically independent.

SNRs for Different Multi-Antenna Modes: For SIMO ($N_t = 1$ and $N_r \geq 1$) with maximal ratio combining, the instantaneous SNR γ_{kn} is given by

$$\gamma_{kn} = \frac{P_T \sum_{j=1}^{N_r} |H_{kn}(1,j)|^2}{\sigma^2}, \tag{1}$$

where P_T is the transmit power of the BS per subband and σ^2 is the additive white Gaussian noise power per subband. It is a gamma RV with PDF $f_{\gamma_{kn}}(v) = \frac{v^{d_k-1} e^{-\frac{v}{\lambda_k}}}{\Gamma(d_k)\lambda^{d_k}}$, for $v \geq 0$, where $\Gamma(d_k) = \int_0^\infty x^{d_k-1} e^{-x}\, dx$ is the gamma function [11, (8.310)]. The PDF has a shape parameter $d_k = N_r$ and a scale parameter $\lambda_k = \frac{P_T \delta x_k^{-\alpha}}{\sigma^2}$ [12]. Similarly, for MISO with maximal ratio transmission, γ_{kn} is a gamma RV with parameters $d_k = N_t$ and $\lambda_k = \frac{P_T \delta x_k^{-\alpha}}{\sigma^2}$. For single-stream MIMO ($N_t \geq 2$ and $N_r \geq 2$), γ_{kn} can be accurately approximated as a gamma RV with $d_k = N_t N_r$ and $\lambda_k = \frac{P_T \delta x_k^{-\alpha}}{\sigma^2} \left(\frac{N_t + N_r}{N_t N_r + 1} \right)^{\frac{2}{3}}$ [12].

A. AMC Using Differential CQI Feedback

The BS has available to it an *MCS set* $\mathcal{M} = \{1, 2, \ldots, M\}$ of MCSs to choose from. MCS m has a rate R_m and a threshold T_m. A transmission using MCS m on subband n for user k succeeds only if $\gamma_{kn} \geq T_m$. Else, an outage occurs [9], [13]. Without loss of generality, let $0 = R_1 < R_2 < \cdots < R_M$ and $0 = T_1 < T_2 < \cdots < T_M < T_{M+1} = \infty$. In conventional AMC, the BS sets the MCS $\tilde{S}_{kn}$ for subband n for user k as m if $T_m \leq \gamma_{kn} < T_{m+1}$. We now describe the differential feedback scheme of LTE and contrast it with full CSI feedback.

1) Full CSI Feedback: In it, a user feeds back the MCS that it can reliably receive on each subband using $B = \log_2(M)$ bits per subband, resulting in a feedback overhead of $N_{\text{SB}} B$ bits per user. In LTE, M is set as 16 [1, Table 10.1].

2) Differential Feedback: It involves the following 2 steps:

Step 1) Wideband CQI Generation: The MCS corresponding to this CQI must be such that a codeword transmitted using it over the entire system bandwidth can be decoded by the user. Since different subbands see different SNRs, it is not obvious at first sight as to which MCS should be chosen.

To do this systematically, we use EESM, whose accuracy has been extensively validated in literature [13], [14] and which has also been used in system-level simulations of LTE [15]. It maps a vector of subband SNRs $\boldsymbol{\gamma}_k = (\gamma_{k1}, \ldots, \gamma_{kN_{\text{SB}}})$ seen by the codeword into a single effective

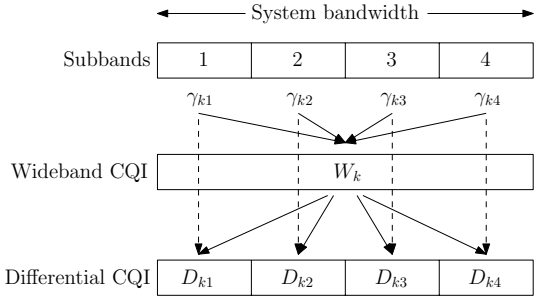

Fig. 1. Illustration of generation of wideband CQI and differential CQI for $N_{\text{SB}} = 4$ subbands for user k.

SNR $\zeta_k^{(m)}$ [14]. For MCS m, it computes $\zeta_k^{(m)}$ as:

$$\zeta_k^{(m)} = -\beta_m \log\left(\frac{1}{N_{\text{SB}}}\sum_{n=1}^{N_{\text{SB}}} \exp\left(-\frac{\gamma_{kn}}{\beta_m}\right)\right), \qquad (2)$$

where β_m is an MCS-dependent constant [14]. Here, $\zeta_k^{(m)}$ is the equivalent SNR for MCS m in a frequency-flat AWGN channel that results in the same probability of error as that when transmitting over the frequency-selective channel.

Since $\zeta_k^{(m)}$ is the equivalent flat-fading SNR for user k, W_k is chosen as the highest rate MCS that has $\zeta_k^{(m)} \geq T_m$. Thus $W_k = m$, for some $m \in \{2, 3, \ldots, M\}$, if and only if $\zeta_k^{(m)} \geq T_m, \zeta_k^{(m+1)} < T_{m+1}, \ldots, \zeta_k^{(M)} < T_M$.

Step 2) Differential CQI Generation: Let $S_{kn} \in \mathcal{M}$ denote the MCS that user k can reliably receive on subband n. Clearly, $S_{kn} = m$ if $T_m \leq \gamma_{kn} < T_{m+1}$. It is encoded differentially with respect to W_k to generate a subband differential CQI offset value D_{kn} as follows [1, Chap. 10]:

$$D_{kn} = \begin{cases} -1, & S_{kn} - W_k \leq -1, \\ 0, & S_{kn} - W_k = 0, \\ 1, & S_{kn} - W_k = 1, \\ 2, & S_{kn} - W_k \geq 2. \end{cases} \qquad (3)$$

The vector $\mathbf{D}_k = (D_{k1}, \ldots, D_{kN_{\text{SB}}})$ of differential CQI offset values, which requires $2N_{\text{SB}}$ bits, and W_k, which requires 4 bits, are then fed back to the BS. This is shown in Figure 1. Thus, at any time, the only MCS indices that user k can report to the BS are $\{W_k - 1, W_k, W_k + 1, W_k + 2\}$.

Given D_{kn} and W_k, the BS transmits with MCS $\tilde{S}_{kn}$ to user k on subband n, where

$$\tilde{S}_{kn} = W_k + D_{kn}. \qquad (4)$$

III. Throughput Analysis

We now analyze the throughput of the differential feedback scheme. We first analyze the single-user scenario. We then analyze the more involved multi-user scenario with scheduling.

A. Single-user Scenario

1) Preliminaries: The fading-averaged throughput $\bar{R}_{kn}$ of a user k on subband n is given by

$$\bar{R}_{kn} = \sum_{m=1}^{M} R_m \Pr\left(\tilde{S}_{kn} = m, \gamma_{kn} \geq T_m\right). \qquad (5)$$

From (3) and (4), the BS transmits using MCS $\tilde{S}_{kn} = m$ when one of the following four mutually exclusive events occurs: (i) $W_k = m + 1, S_{kn} \leq m$; (ii) $W_k = m, S_{kn} = m$; (iii) $W_k = m - 1, S_{kn} = m$; or (iv) $W_k = m - 2, S_{kn} \geq m$. Therefore, it follows from the law of total probability that

$$\begin{aligned} &\Pr\left(\tilde{S}_{kn} = m, \gamma_{kn} \geq T_m\right) \\ &\quad = \Pr(W_k = m+1, S_{kn} \leq m, \gamma_{kn} \geq T_m) \\ &\qquad + \Pr(W_k = m, S_{kn} = m, \gamma_{kn} \geq T_m) \\ &\qquad + \Pr(W_k = m-1, S_{kn} = m, \gamma_{kn} \geq T_m) \\ &\qquad + \Pr(W_k = m-2, S_{kn} \geq m, \gamma_{kn} \geq T_m). \end{aligned} \qquad (6)$$

The event in the the first probability term in (6) is equivalent to $\zeta_k^{(m+1)} \geq T_{m+1}$, $\zeta_k^{(m+2)} < T_{m+2}, \ldots, \zeta_k^{(M)} < T_M$, and $T_m \leq \gamma_{kn} < T_{m+1}$. Computing its probability requires an $M - m$ dimensional joint PDF of the RVs $\zeta_k^{(m+1)}, \ldots, \zeta_k^{(M)}$ and γ_{kn}, for which no expression is known. In fact, an exact closed-form expression is not available even for the marginal PDF of $\zeta_k^{(m)}$. Moreover, the RVs $\zeta_k^{(1)}, \zeta_k^{(2)}, \ldots, \zeta_k^{(M)}$ are correlated since they are all functions of the same set of RVs $\gamma_{k1}, \ldots, \gamma_{kN_{\text{SB}}}$.

To tackle this problem, we use the following intuition. If an MCS m cannot be decoded by the user, then it it is highly unlikely that a higher rate MCS can be decoded. Therefore,

$$\begin{aligned} &\Pr\big(\zeta_k^{(m+1)} \geq T_{m+1}, \zeta_k^{(m+2)} < T_{m+2}, \ldots, \zeta_k^{(M)} < T_M, \\ &\qquad\qquad T_m \leq \gamma_k < T_{m+1}\big) \\ &\quad \approx \Pr\big(\zeta_k^{(m+1)} \geq T_{m+1}, \zeta_k^{(m+2)} < T_{m+2}, \\ &\qquad\qquad T_m \leq \gamma_{kn} < T_{m+1}\big). \end{aligned} \qquad (7)$$

Using the law of total probability, we then have

$$\begin{aligned} &\Pr\left(\zeta_k^{(m+1)} \geq T_{m+1}, \zeta_k^{(m+2)} < T_{m+2}, T_m \leq \gamma_{kn} < T_{m+1}\right) \\ &\quad = \Pr\left(\zeta_k^{(m+1)} \geq T_{m+1}, T_m \leq \gamma_{kn} < T_{m+1}\right) \\ &\qquad - \Pr\left(\zeta_k^{(m+1)} \geq T_{m+1}, \zeta_k^{(m+2)} \geq T_{m+2}, \right. \\ &\qquad\qquad \left. T_m \leq \gamma_{kn} < T_{m+1}\right). \end{aligned} \qquad (8)$$

Using the same intuition as above to simplify the second probability term in (8) yields

$$\begin{aligned} &\Pr\left(\zeta_k^{(m+1)} \geq T_{m+1}, \zeta_k^{(m+2)} \geq T_{m+2}, T_m \leq \gamma_{kn} < T_{m+1}\right) \\ &\quad \approx \Pr\left(\zeta_k^{(m+1)} \geq T_{m+1}, T_m \leq \gamma_{kn} < T_{m+1}\right) \\ &\qquad - \Pr\left(\zeta_k^{(m+2)} \geq T_{m+2}, T_m \leq \gamma_{kn} < T_{m+1}\right). \end{aligned} \qquad (9)$$

Similarly, the other probability terms in (6) are given by

$$\begin{aligned} &\Pr\big(W_k = m, S_{kn} = m, \gamma_{kn} \geq T_m\big) \\ &\quad \approx \Pr\big(\zeta_k^{(m)} \geq T_m, T_m \leq \gamma_{kn} < T_{m+1}\big) \\ &\qquad - \Pr\big(\zeta_k^{(m+1)} \geq T_{m+1}, T_m \leq \gamma_{kn} < T_{m+1}\big), \end{aligned} \qquad (10)$$

$$\begin{aligned} &\Pr\big(W_k = m-1, S_{kn} = m, \gamma_{kn} \geq T_m\big) \\ &\quad \approx \Pr\big(\zeta_k^{(m-1)} \geq T_{m-1}, T_m \leq \gamma_{kn} < T_{m+1}\big) \\ &\qquad - \Pr\big(\zeta_k^{(m)} \geq T_m, T_m \leq \gamma_{kn} < T_{m+1}\big), \end{aligned} \qquad (11)$$

$$\Pr\big(W_k = m-2, S_{kn} \geq m, \gamma_{kn} \geq T_m\big) \approx \Pr\big(\zeta_k^{(m-2)} \geq T_{m-2}, \gamma_{kn} \geq T_m\big) - \Pr\big(\zeta_k^{(m-1)} \geq T_{m-1}, \gamma_{kn} \geq T_m\big). \quad (12)$$

Combining these simplifies (6) considerably and yields

$$\Pr\Big(\tilde{S}_{kn} = m, \gamma_{kn} \geq T_m\Big) \approx \Pr\big(\zeta_k^{m-2} \geq T_{m-2}, \gamma_{kn} \geq T_m\big) - \Pr\big(\zeta_k^{m-1} \geq T_{m-1}, \gamma_{kn} \geq T_{m+1}\big) - \Pr\Big(\zeta_k^{(m+2)} \geq T_{m+2}, \gamma_{kn} \geq T_m\Big) + \Pr\Big(\zeta_k^{(m+2)} \geq T_{m+2}, \gamma_{kn} \geq T_{m+1}\Big). \quad (13)$$

General Form: Each term in (13) is of the form $\Pr\Big(\zeta_k^{(l)} \geq T_l, \gamma_{kn} \geq t\Big)$, where $l \in \{m-2, m-1, m+2\}$ and $t \in \{T_m, T_{m+1}\}$. It can be written in terms of the PDF $f_{\gamma_{kn}}(\cdot)$ of γ_{kn} as

$$\Pr\Big(\zeta_k^{(l)} \geq T_l, \gamma_{kn} \geq t\Big) = \int_t^\infty f_{\gamma_{kn}}(r) \Pr\Big(\zeta_k^{(l)} \geq T_l \,|\, \gamma_{kn} = r\Big)\, dr. \quad (14)$$

From the definition of $\zeta_k^{(l)}$ in (2), we have

$$\Pr\Big(\zeta_k^{(l)} \geq T_l \,|\, \gamma_{kn} = r\Big) = \Pr\left(-\beta_l \log\left(\frac{1}{N_{\text{SB}}} \sum_{j=1}^{N_{\text{SB}}} e^{-\frac{\gamma_{kj}}{\beta_l}}\right) \geq T_l \,\middle|\, \gamma_{kn} = r\right). \quad (15)$$

Rearranging terms and using the fact that the RVs $\gamma_{k1}, \ldots, \gamma_{k(n-1)}, \gamma_{k(n+1)}, \ldots, \gamma_{kN_{\text{SB}}}$ are statistically independent of γ_{kn}, it can be shown that

$$\Pr\Big(\zeta_k^{(l)} \geq T_l \,|\, \gamma_{kn} = r\Big) = F_{X_l}(x_l(r)), \quad (16)$$

where $x_l(r) = (N_{\text{SB}} e^{\frac{-T_l}{\beta_l}} - e^{\frac{-r}{\beta_l}})/(N_{\text{SB}} - 1)$ and

$$X_l = \frac{1}{N_{\text{SB}} - 1} \sum_{j=1, j\neq n}^{N_{\text{SB}}} e^{-\frac{\gamma_{kj}}{\beta_l}}. \quad (17)$$

Evaluating CDF of X_l: While an exact expression for $F_{X_l}(\cdot)$ is not available, it has been shown in [13] that X_l, which is related to the effective SNR of MCS l over $N_{\text{SB}} - 1$ subbands, is well approximated as a Beta RV.[1] Thus,

$$F_{X_l}(x) = \mathcal{B}(x; a_l, b_l), \text{ for } x \in [0, 1], \quad (18)$$

where $\mathcal{B}(x; a_l, b_l) = \frac{\int_0^x z^{a_l-1}(1-z)^{b_l-1}\, dz}{\int_0^1 z^{a_l-1}(1-z)^{b_l-1}\, dz}$ is the regularized incomplete Beta function [11, (8.392)]. The parameters a_l and b_l are given in terms of the mean μ_l and variance v_l of X_l by

$$a_l = \mu_l \left(\mu_l - \mu_l^2 - v_l\right)/v_l, \quad (19)$$

$$b_l = (1 - \mu_l)\left(\mu_l - \mu_l^2 - v_l\right)/v_l. \quad (20)$$

From (17), it can be shown that

$$\mu_l = (1 + d_k \lambda_k \beta_l^{-1})^{-d_k}, \quad (21)$$

$$v_l = \left((1 + 2\beta_l^{-1} d_k \lambda_k)^{-d_k} - \mu_l^2\right)/\left(N_{\text{SB}} - 1\right). \quad (22)$$

Substituting (21) and (22) in (19) and (20) yields a_l and b_l.

Final Simplifications: Substituting the Gamma PDF $f_{\gamma_{kn}}(r)$ and (16) in (14) yields

$$\Pr\Big(\zeta_k^{(l)} \geq T_l, \gamma_{kn} \geq t\Big) = \int_t^\infty \frac{r^{d_k-1} e^{-\frac{r}{\lambda_k}}}{\Gamma(d_k)\, \lambda_k^{d_k}} \mathcal{B}(x_l(r); a_l, b_l)\, dr. \quad (23)$$

As shown in Appendix A, this can be evaluated as

$$\Pr\Big(\zeta_k^{(l)} \geq T_l, \gamma_{kn} \geq t\Big) = \frac{e^{\frac{-t}{\lambda_k}}}{\Gamma(d_k)} \sum_{i_1=0}^{d_k-1} \binom{d_k - 1}{i_1} \left(\frac{t}{\lambda_k}\right)^{i_1} \times \sum_{i_2=0}^{Q} w(d_k - 1, i_2) \mathcal{B}\left(x_l(\lambda_k \theta(d_k - 1, i_2) + t); a_l, b_l\right), \quad (24)$$

where $w(.,.)$ and $\theta(.,.)$ are the Q weights and abscissas, respectively, of generalized Gauss-Laguerre quadrature [17]. Recall that λ_k and d_k depend on the multi-antenna mode used. In (24), we have found that just $Q = 8$ terms are sufficient for ensuring numerical accuracy for a wide range of the parameters of interest.

Evaluating (23) for all the values of l and t that arise in (13) and combining them yields $\Pr\Big(\tilde{S}_{kn} = m, \gamma_{kn} \geq T_m\Big)$. Thereafter, substituting it in (5) yields the final expression for $\bar{R}_{kn}$.

B. Multi-user Scenario

We now analyze the cell throughput per subband when there are K users in the cell and the BS employs the RR scheduler. It allocates subbands to users in a periodic manner such that each user is scheduled once in a period. Hence, it is fair. Since the fading is assumed to be flat within a subband, the entire subband is assigned to a user.

Let u denote the scheduled user on subband n. Recall that $\tilde{S}_{un}$ denotes the MCS that the BS uses to transmit to user u on subband n. Thus, the cell throughput on subband n is given as follows.

Result *1:* The cell throughput $\bar{R}_{\text{cell}}(n)$ on subband n when the RR scheduler is employed by the BS is given by

$$\bar{R}_{\text{cell}}(n) = \frac{1}{K} \sum_{k=1}^{K} \sum_{m=1}^{M} R_m \Pr\Big(\tilde{S}_{kn} = m, \gamma_{kn} \geq T_m\Big), \quad (25)$$

where the expression for $\Pr\big(\tilde{S}_{kn} = m, \gamma_{kn} \geq T_m\big)$ is derived in Section III-A.

[1] The Beta approximation for X_l is based on the fact that $e^{-\frac{\gamma_{kj}}{\beta_l}}$ has a finite and positive support of $[0, 1]$. When N such i.i.d. RVs with finite and positive support are added, the central limit approximation of Papoulis states that the sum is well approximated by a Beta RV [16].

Proof: It follows from first principles and the law of total expectation. It is based on the fact that only one user is scheduled at a time on a subband. ■

The above approach can also be generalized to other schedulers such as the greedy and proportional fair schedulers.

C. Fully Correlated Subbands Scenario

To understand the sensitivity of the throughput to the correlation between the subband SNRs, we now analyze the other extreme case in which all the subbands for user k are correlated with correlation coefficient equal to 1. This corresponds to the coherence bandwidth being equal to the system bandwidth. For this case, the following results can be shown along lines similar to those in Sections III-A and III-B.

For the single-user scenario, the average throughput $\bar{R}_{kn}$ can be shown to be

$$\bar{R}_{kn} = \sum_{m=1}^{M} R_m \left[L\left(\frac{T_{m+1}}{\lambda_k}, d_k\right) - L\left(\frac{T_m}{\lambda_k}, d_k\right)\right], \quad (26)$$

where $L(y, d_k) = \frac{1}{\Gamma(d_k)} \int_0^y x^{d_k-1} e^{-x}\, dx$ denotes the lower incomplete gamma function [11]. Similarly, for the multi-user scenario, the cell throughput $\bar{R}_{\text{cell}}(n)$ for subband n is

$$\bar{R}_{\text{cell}}(n) = \frac{1}{K} \sum_{k=1}^{K} \bar{R}_{kn}. \quad (27)$$

IV. Simulation Results and Comparisons

We now present Monte Carlo simulation results that characterize the throughput of the differential feedback scheme under a wide range of system parameter settings. We first systematically verify the accuracy of modeling X_l as a Beta RV. We then compare the analysis and the simulation throughput results for both single-user and multi-user scenarios.

Simulation Set Up and Parameters: The MCS set is as per LTE [1, Table 10.1]. It has $M = 16$ MCSs whose rates range from 0 to 5.55 bits/symbol. The associated MCS thresholds are generated as $T_m = (2^{R_m} - 1)/\eta$, where η is the coding loss factor. It is set as 0.398 [3]. The values of β_l for different MCSs are specified in [18].

In the multi-user scenario, we generate 50 independent drops of K users, whose locations are distributed uniformly in a cell of radius $r_c = 1$ km. For each drop, we generate 2000 fade realizations for each user. The simulation results are averaged over the fades and the user drops. The transmit power P_T is set such that the cell-edge SNR is P_{edge}. The noise power spectral density is -174 dBm/Hz. The path loss parameters are set as $\alpha = 3.5$ and $\delta = 10^{-3}$. A subband consists of $q = 4$ PRBs. The analysis results are calculated using the expressions derived in Section III for each user drop. These are then numerically averaged over the drops.

Accuracy of Approximating X_l as a Beta RV: To assess the accuracy, we compare the CDF and the complementary CDF (CCDF) of the Beta RV with the empirical CDF and CCDF of X_l. The CDF captures the accuracy of the fit for low values of X_l, but it saturates to 1 at large values for all PDFs. Similarly, the CCDF captures better the accuracy at high values of X_l. Such a comparison methodology has also been used in [3], [13].

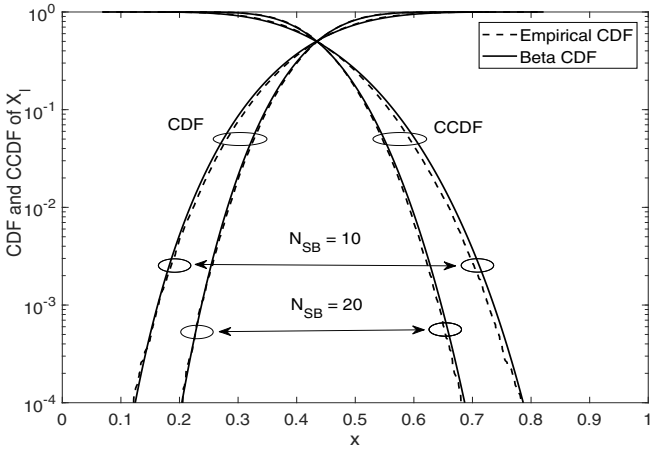

Fig. 2. CDF and CCDF of X_l for i.i.d. subbands for SISO for $N_{\text{SB}} = 10$ and 20 ($l = 11$ and $\bar{\gamma}_k = 10$ dB).

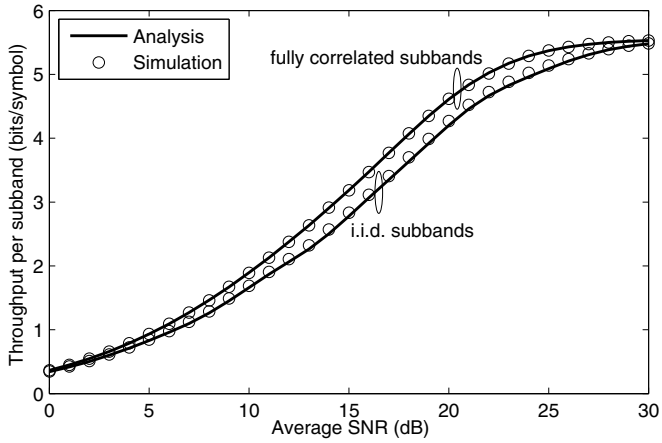

Fig. 3. Single-user scenario: Throughput per subband for a user as a function of average SNR for SIMO ($N_{\text{SB}} = 10$, $K = 1$, $N_t = 1$, $N_r = 2$).

Figure 2 plots the CDF and CCDF of X_l for MCS $l = 11$, which uses 64 QAM and a 0.46 rate code, at an average SNR of $\bar{\gamma}_k = 10$ dB for SISO. Results are shown for $N_{\text{SB}} = 10$ and 20 subbands. We see that the approximation is accurate over a four orders of magnitude range. Also, for both CDF and CCDF, we observe that the accuracy of the fit increases as N_{SB} increases. This is because the central limit approximation of Papoulis [16], which motivated the Beta distribution, becomes more accurate as N_{SB} increases.

Single-user Scenario: Figure 3 plots the throughput per subband of a user as a function of the average SNR $\bar{\gamma}_k$ for SIMO ($N_t = 1$, $N_r = 2$) when the subband SNRs are i.i.d. Also shown for comparison are the corresponding results when the subband SNRs are fully correlated. We observe an excellent fit between the analytical and simulation results for all SNRs. The throughput increases as $\bar{\gamma}_k$ increases in both cases. The throughput when the subband SNRs are fully

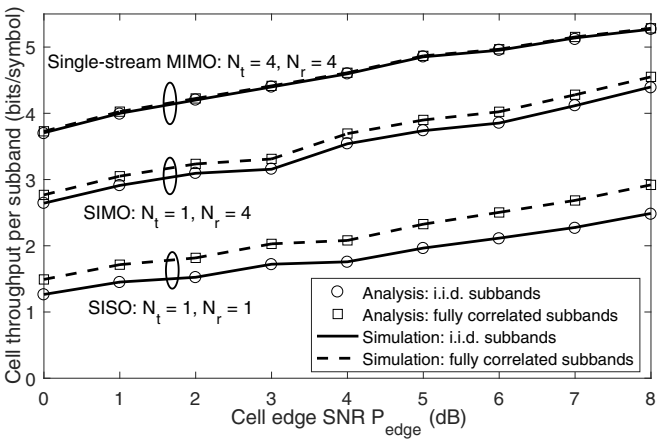

Fig. 4. Multi-user scenario: Cell throughput as a function of P_{edge} for SISO, SIMO, and single-stream MIMO for the RR scheduler ($N_{\text{SB}} = 10$, $K = 10$).

correlated is higher than when they are i.i.d. This is because in the former case, the wideband MCS is the same as the MCS for each subband of the user. Hence, it is as good as having full CSI. Compared to full CSI, the loss in throughput due to the use of differential feedback is 12.27% at $\bar{\gamma}_k = 10$ dB and 7.40% at $\bar{\gamma}_k = 20$ dB.

Multi-user Scenario with Scheduling: Figure 4 plots the cell throughput for 10 users, which is averaged over both user locations and fades, as a function of the cell-edge SNR P_{edge}. Results are shown for SISO ($N_t = 1$, $N_r = 1$), SIMO ($N_t = 1$, $N_r = 4$), and single-stream MIMO ($N_t = 4$, $N_r = 4$) for the RR scheduler. The corresponding results for MISO ($N_t = 4$, $N_r = 1$) are the same as for SIMO and are not shown. Again, we observe an excellent match between the analysis and simulation results. The cell throughput increases as P_{edge} increases. As in the single-user scenario, it is higher when the subbands are fully correlated than when they are i.i.d. The reduction in throughput due to differential feedback for the range of cell-edge SNRs considered is 15.0% for SISO, 4.2% for SIMO, and 0.3% for single-stream MIMO. This is small given the significant reduction in the feedback overhead that is achieved by differential feedback.

V. Conclusions

We proposed a novel and accurate model and analysis of the eNodeB-configured subband feedback scheme in LTE that employs differential feedback. We derived the expressions for throughput for different multi-antenna modes for the single-user and multi-user scenarios when the subband SNRs of a user are i.i.d. For this, we modeled the generation of the wideband and differential CQIs using EESM. For comparison, we also analyzed the other extreme scenario in which the subband SNRs of a user are fully correlated and in which differential feedback is as good as having full CSI. We observed that differential feedback markedly reduces the feedback overhead while incurring only a marginal reduction in the throughput. Future work involves generalizing the analysis to a multi-cell, multi-user scenario with co-channel interference.

Appendix

A. Evaluating $Pr\left(\zeta_k^{(l)} \geq T_l, \gamma_{kn} \geq t\right)$

To evaluate (23), we use the transformation $v = \frac{r}{\lambda_k} - \frac{t}{\lambda_k}$ and then do a binomial series expansion of the $(v + t/\lambda_k)^{d_k - 1}$ term that arises in the integrand. This yields

$$\int_t^{\infty} \frac{r^{d_k-1} e^{-\frac{r}{\lambda_k}}}{\Gamma(d_k)\,\lambda_k^{d_k}} \mathcal{B}\left(x_l(r); a_l, b_l\right)\, dr = \frac{e^{\frac{-t}{\lambda_k}}}{\Gamma(d_k)} \sum_{i_1=0}^{d_k-1} \binom{d_k-1}{i_1}$$

$$\times \left(\frac{t}{\lambda_k}\right)^{i_1} \int_0^{\infty} v^{d_k-1-i_1} e^{-v} \mathcal{B}\left(x_l(\lambda_k v + t); a_l, b_l\right)\, dv. \quad (28)$$

Approximating $\int_0^{\infty} v^{d_k-1-i_1} e^{-v} \mathcal{B}\big(x_l(\lambda_k v + t); a_l, b_l\big)\, dv$ using generalized Gauss-Laguerre quadrature [17] yields (24).

References

[1] S. Sesia, I. Toufik, and M. Baker, *LTE – The UMTS Long Term Evolution, From Theory to Practice*, 2nd ed. John Wiley and Sons, 2009.

[2] D. J. Love, R. W. Heath, V. K. N. Lau, D. Gesbert, B. D. Rao, and M. Andrews, "An overview of limited feedback in wireless communication systems," *IEEE J. Sel. Areas Commun.*, vol. 26, no. 8, pp. 1341–1365, Oct. 2008.

[3] S. N. Donthi and N. B. Mehta, "Joint performance analysis of channel quality indicator feedback schemes and frequency-domain scheduling for lte," *IEEE Trans. Veh. Technol.*, vol. 60, no. 7, pp. 3096–3109, Sep. 2011.

[4] J. Leinonen, J. Hamalainen, and M. Juntti, "Performance analysis of downlink OFDMA resource allocation with limited feedback," *IEEE Trans. Wireless Commun.*, vol. 8, no. 6, pp. 2927–2937, Jun. 2009.

[5] J. Chen, R. A. Berry, and M. L. Honig, "Limited feedback schemes for downlink OFDMA based on sub-channel groups," *IEEE J. Sel. Areas Commun.*, vol. 26, no. 8, pp. 1451–1461, Oct. 2008.

[6] J. C. Ikuno, "System level modeling and optimization of the LTE downlink," Ph.D. Dissertation, TU Wien, Vienna, Austria, Mar. 2012.

[7] H. J. G. Torres and B. M. Roberto, "Analysis of the effects of CQI feedback for LTE networks on ns-3," in *Proc. IEEE Latin-America Conf. on Commun. (LATINCOM)*, Nov. 2014, pp. 1–6.

[8] N. Shojaedin, M. Ghaderi, and A. Sridharan, "Effect of handover on the performance of scheduling algorithms in LTE networks," in *Proc. WCNC*, Mar. 2015, pp. 1386–1391.

[9] M. Lopez-Bentez, "Throughput performance models for adaptive modulation and coding under fading channels," in *Proc. WCNC*, Apr. 2016, pp. 1–6.

[10] A. J. Goldsmith, *Wireless Communications*, 2nd ed. Cambridge Univ. Press, 2005.

[11] I. S. Gradshteyn and I. M. Ryzhik, *Table of Integrals, Series and Products*, 4th ed. Academic Press, 1980.

[12] Y. Li, L. Zhang, L. J. Cimini, and H. Zhang, "Statistical analysis of MIMO beamforming with co-channel unequal-power MIMO interferers under path-loss and Rayleigh fading," *IEEE Trans. Signal Process.*, vol. 59, no. 8, pp. 3738–3748, Aug. 2011.

[13] J. Francis and N. B. Mehta, "EESM-based link adaptation in point-to-point and multi-cell OFDM systems: Modeling and analysis," *IEEE Trans. Wireless Commun.*, vol. 13, no. 1, pp. 407–417, Jan. 2014.

[14] E. Westman, "Calibration and evaluation of the exponential effective SINR mapping (EESM) in 802.16," Master's thesis, Royal Institute of technology (KTH), Stockholm, Sweden, Sep. 2006.

[15] J. C. Ikuno, M. Wrulich, and M. Rupp, "System level simulation of LTE networks," in *Proc. VTC (Spring)*, May 2010, pp. 1–5.

[16] A. Papoulis, *The Fourier Integral and its Applications*, 1st ed. Mcgraw-Hill, 1962.

[17] P. Rabinowitz and G. Weiss, "Tables of abscissas and weights for numerical evaluation of integrals of the form $\int_0^{\infty} x^n e^{-x} f(x)\, dx$," *Mathematical Tables and Other Aids to Computation*, vol. 13, no. 68, pp. 285–294, Oct. 1959.

[18] J. Fan, Q. Yin, G. Y. Li, B. Peng, and X. Zhu, "MCS selection for throughput improvement in downlink LTE systems," in *Proc. Int. Conf. Comp. Commun. and Netw.*, Jul. 2011, pp. 1–5.